

1 Satellite-based Estimation of the Impacts of Summertime Wildfires on  
2 PM<sub>2.5</sub> concentration in United States

3 Zhixin Xue<sup>1</sup>, Pawan Gupta<sup>2,3</sup>, and Sundar Christopher<sup>1</sup>

4 <sup>1</sup>Department of Atmospheric and Earth Science, The University of Alabama in Huntsville,  
5 Huntsville, 35806 AL, USA

6 <sup>2</sup>STI, Universities Space Research Association (USRA), Huntsville, 35806 AL, USA

7 <sup>3</sup>NASA Marshall Space Flight Center, Huntsville, AL, 35806, USA

8 **Abstract**

9 Frequent and widespread wildfires in North Western United States and Canada has become  
10 the “*new normal*” during the northern hemisphere summer months, which significantly degrades  
11 particulate matter air quality in the United States. Using the mid-visible Multi Angle  
12 Implementation of Atmospheric Correction (MAIAC) satellite-derived Aerosol Optical Depth  
13 (AOD) with meteorological information from the European Centre for Medium-Range Weather  
14 Forecasts (ECMWF) and other ancillary data, we quantify the impact of these fires on fine  
15 particulate matter concentration (PM<sub>2.5</sub>) air quality in the United States. We use a Geographically  
16 Weighted Regression method to estimate surface PM<sub>2.5</sub> in the United States between low (2011)  
17 and high (2018) fire activity years. Our results indicate that smoke aerosols caused significant  
18 pollution changes over half of the United States. We estimate that nearly 29 states have increased  
19 PM<sub>2.5</sub> during the fire active year and 15 of these states have PM<sub>2.5</sub> concentrations more than 2  
20 times than that of the inactive year. Furthermore, these fires increased the daily mean surface PM<sub>2.5</sub>  
21 concentrations in Washington and Oregon by 38 to 259 μg m<sup>-3</sup> posing significant health risks  
22 especially to vulnerable populations. Our results also show that the GWR model can be

23 successfully applied to PM<sub>2.5</sub> estimations from wildfires thereby providing useful information for  
24 various applications including public health assessment.

## 25 **1. Introduction**

26 The United States (US) Clean Air Act (CAA) was passed in 1970 to reduce pollution levels  
27 and protect public health that has led to significant improvements in air quality (Hubbell et al.,  
28 2010; Samet, 2011). However, the northern part of the US continues to experience an increase in  
29 surface PM<sub>2.5</sub> due to fires in North Western United States and Canada (hereafter NWUSC)  
30 especially during the summer months and these aerosols are a new source of ‘pollution’ (Coogan  
31 et al., 2019; Dreessen et al., 2016). The smoke aerosols from these fires increase fine particulate  
32 matter (PM<sub>2.5</sub>) concentrations and degrade air quality in the United States (Miller et al., 2011).  
33 Moreover several studies have shown that from 2013 to 2016, over 76% of Canadians and 69% of  
34 Americans were at least minimally affected by wildfire smoke (Munoz-Alpizar et al., 2017).  
35 Although wildfire pre-suppression and suppression costs have increased, the number of large fires  
36 and the burnt areas in many parts of western Canada and the United States have also increased.  
37 (Hanes et al., 2019; Tymstra et al., 2019). Furthermore, in a changing climate, as surface  
38 temperature increases and humidity decreases, the flammability of land cover also increases, and  
39 thus accelerate the spread of wildfires (Melillo et al., 2014). The accumulation of flammable  
40 materials like leaf litter can potentially trigger severe wildfire events even in those forests that  
41 hardly experience wildfires (Calkin et al., 2015; Hessburg et al., 2015; Stephens, 2005).

42 Wildfire smoke exposure can cause small particles to be lodged in lungs that may lead to  
43 exacerbations of asthma chronic obstructive pulmonary disease (COPD), bronchitis, heart disease  
44 and pneumonia (Apte et al., 2018; Cascio, 2018). According to a recent study, a 10  $\mu\text{gm}^{-3}$   
45 increase in PM<sub>2.5</sub> is associated with a 12.4% increase in cardiovascular mortality (Kollanus et al.,

46 2016). In addition, exposure to wildfire smoke is also related to massive economic costs due to  
47 premature mortality, loss of workforce productivity, impacts on the quality of life and  
48 compromised water quality (Meixner and Wohlgemuth, 2004).

49 Surface  $PM_{2.5}$  is one of the most commonly used parameters to assess the health effects of  
50 ambient air pollution. Given the sparsity of measurements in many parts of the world, it is not  
51 possible to use interpolation techniques between monitors to provide  $PM_{2.5}$  estimates on a square  
52 kilometer basis. Since surface monitors are limited, satellite data has been used with numerous  
53 ancillary data sets to estimate surface  $PM_{2.5}$  at various spatial scales. Several techniques have been  
54 developed to estimate surface  $PM_{2.5}$  using satellite observations from regional to global scales  
55 including simple linear regression, multiple linear regression, mixed-effect model, chemical  
56 transport model (scaling methods), geographically weighted regression (GWR), and machine  
57 learning methods (see Hoff and Christopher, 2009 for a review). The commonly used global  
58 satellite data product is the 550nm (mid-visible) aerosol optical depth (AOD) which is a unitless  
59 columnar measure of aerosol extinction. Simple linear regression method uses satellite AOD as  
60 the only independent variable, which shows limited predictability compared to other methods and  
61 correlation coefficients vary from 0.2 to 0.6 from the Western to Eastern United States (Zhang et  
62 al., 2009). Multiple linear regression method uses meteorological variables along with AOD data,  
63 and the prediction accuracy varies with different conditions including the height of boundary layer  
64 and other meteorological conditions (Goldberg et al., 2019; Gupta and Christopher, 2009b; Liu et  
65 al., 2005). For both univariate model and multi-variate models, AOD shows stronger correlation  
66 with  $PM_{2.5}$  during-fire episodes compared to pre-fire and post-fire periods (Mirzaei et al., 2018).  
67 Chemistry transport models (CTM) that scale the satellite AOD by the ratio of  $PM_{2.5}$  to AOD  
68 simulated by models can provide  $PM_{2.5}$  estimations without ground measurements, which are

69 different than other statistical methods (Donkelaar et al., 2019, 2006). However, the CTM models  
70 that depend on reliable emission data usually show limited predictability at shorter time scales,  
71 and is largely useful for studies that require annual averages (Hystad et al., 2012).

72 The relationship among  $PM_{2.5}$ , AOD and other meteorological variables is not spatially  
73 consistent (Hoff and Christopher, 2009; Hu, 2009). Therefore, methods that consider spatial  
74 variability can replicate surface  $PM_{2.5}$  with higher accuracy. One such method is the GWR, which  
75 is a non-stationary technique that models spatially varying relationships by assuming that the  
76 coefficients in the model are functions of locations (Brunsdon et al., 1996; Fotheringham et al.,  
77 1998, 2003). In 2009, satellite-retrieved AOD was introduced in the GWR method to predict  
78 surface  $PM_{2.5}$  (Hu, 2009) followed by the use of meteorological parameters and land use  
79 information (Hu et al., 2013). Meteorological variables are crucial for simulating surface  $PM_{2.5}$   
80 since they interact with  $PM_{2.5}$  through different processes which will be discussed in detail in the  
81 data section (Chen et al., 2020). Several studies (Guo et al., 2021; Ma et al., 2014; You et al.,  
82 2016) successfully applied [the GWR](#) model in estimating  $PM_{2.5}$  in China by using AOD and  
83 meteorological features as predictors. Similar to all the statistical methods, however, the GWR  
84 relies on adequate number and density of surface measurements (Chu et al., 2016; Gu, 2019; Guo  
85 et al., 2021), underscoring the importance of adequate ground monitoring of surface  $PM_{2.5}$ .

86 In this paper, we use satellite data from the Moderate Resolution Imaging  
87 Spectroradiometer (MODIS) and surface  $PM_{2.5}$  data combined with meteorological and other  
88 ancillary information to develop and use the GWR method to estimate  $PM_{2.5}$ . The use of the GWR  
89 method is not novel and we merely use a proven method to ~~apply this towards~~[estimate](#) surface  
90  $PM_{2.5}$  ~~estimations from~~ forest fires. We calculate the change in  $PM_{2.5}$  between a high fire activity  
91 (2018) with low fire activity (2011) periods during summer to assess the role of NWUSC wildfires

Xue, Gupta, Christopher, submitted to Atmospheric Chemistry and Physics

92 on surface  $PM_{2.5}$  in the United States. The paper is organized as follows: We describe the data sets  
93 used in this study followed by the GWR method. We then describe the results and discussion  
94 followed by a summary with conclusions.

95

## 96 **2. Data**

97 A 17-day period (August 9<sup>th</sup> to August 25<sup>th</sup>) in 2018 (high fire activity) and 2011 (low fire  
98 activity) was selected based on analysis of total fires (details in methodology section) to assess  
99 surface  $PM_{2.5}$  (Table 1).

100 **2.1 Ground level  $PM_{2.5}$  observations:** Daily surface  $PM_{2.5}$  from the Environment Protection  
101 Agency (EPA) are used in this study. These data are from Federal Reference Methods (FRM),  
102 Federal Equivalent Methods (FEM), or other methods that are to be used in the National Ambient  
103 Air Quality Standards (NAAQS) decisions. A total of 1003 monitoring sites in the US are included  
104 in our study with 949 having valid observations in the study period in 2018, and a total of 873 sites  
105 with 820 having valid observations in the study period in 2011.  $PM_{2.5}$  values less than  $2 \mu\text{gm}^{-3}$  are  
106 discarded since they are lower than the established detection limit (Hall et al., 2013).

107 **2.2 Satellite Data:** AOD which represents the total column aerosol mass loading is related to  
108 surface  $PM_{2.5}$  as a function of aerosol vertical properties and physical properties (Koelemeijer et  
109 al., 2006):

$$110 \quad AOD = PM_{2.5} H f(RH) \frac{3Q_{\text{ext,dry}}}{4\rho r_{\text{eff}}} = PM_{2.5} H S \quad (1)$$

111 Where H is the aerosol layer height,  $f(RH)$  is the ratio of ambient and dry extinction  
112 coefficients,  $Q_{\text{ext,dry}}$  is the extinction efficiency under dry conditions,  $r_{\text{eff}}$  is the particle effective

113 radius,  $\rho$  is the aerosol mass density and  $S$  is the specific extinction efficiency ( $\text{m}^2 \text{g}^{-1}$ ) of the  
114 aerosol at ambient conditions. Therefore AOD usually has a strong positive correlation with  $\text{PM}_{2.5}$ ,  
115 and the relationship varies depending on other meteorological parameters which will be discussed  
116 in detail in the following section.

117 The MODIS mid visible AOD from the Multi-Angle Implementation of Atmospheric  
118 Correction (MAIAC) product (MCD19A2 Version 6 data product) is used in this study. We used  
119 the MAIAC- retrieved Terra and Aqua MODIS AOD product at 1 km pixel resolution (Lyapustin  
120 et al., 2018). Different orbits are averaged to obtain mean daily values. Since thick smoke plumes  
121 generated by wildfires can be misclassified as cloud, we preserve possible cloud contaminated  
122 pixels to preserve the thick smoke pixels, and only AOD less than 0 will be discarded. Validation  
123 with AERONET studies show that 66% of the MAIAC AOD data agree within  $\pm 0.5 \sim \pm 0.1$  AOD  
124 (Lyapustin et al., 2018). Largely due to cloud cover, grid cells may have limited number of AOD  
125 observations within a certain period. On average, cloud free AOD data are available about 40% of  
126 the time during August 9<sup>th</sup> to August 25<sup>th</sup> in 2018 when fires were active in the region bounded by  
127 25~50°N, 65~125°W. Smoke flag from the same product is used as a predictor in estimating  
128 surface  $\text{PM}_{2.5}$ . The smoke detection is performed using MODIS red, blue and deep blue bands, and  
129 smoke pixels are separated from dust and clouds based on absorption parameter, size parameter  
130 and thermal thresholds (see Lyapustin et al., [2012](#); 2018, ~~2012~~ for further discussion). Smoke flag  
131 data can provide the percentage of smoke pixel in each grid, which is related to smoke coverage.

132 We also use the MODIS level-3 daily FRP (MCD14ML, fire radiative power) product  
133 which combines Terra and Aqua fire products to assess wildfire activity. The fire radiative energy  
134 indicates the rate of combustion and thus FRP can be used for characterizing active fires (Freeborn

135 et al, 2014). For purposes of the study we sum the FRP within every  $2.3^{\circ} \times 3.5^{\circ}$  box to represent  
136 the total fire activity in different locations.

137 **2.3 Meteorological data:** Meteorological information including boundary layer height (BLH), 2m  
138 temperature (T2M), 10m wind speed (WS), surface relative humidity (RH) and surface pressure  
139 (SP) are obtained from the European Centre for Medium-Range Weather Forecasts (ECMWF)  
140 reanalysis (ERA5) product, with a spatial resolution of 0.25 degrees and temporal resolution of 1  
141 hour and is matched temporally with the satellite overpass time. The meteorological parameters  
142 provide important information of different processes affecting surface  $PM_{2.5}$  concentration, which  
143 can also be seen as supplements of the AOD- $PM_{2.5}$  relationship as previously discussed.

144 The BLH can provide information of aerosol layer height (H in equation 1) as aerosols are often  
145 found to be well-mixed within the boundary layer (Gupta and Christopher, 2009b). With same  
146 amount of pollution within the boundary layer, the higher the BLH is, the more  $PM_{2.5}$  is distributed  
147 within that layer and vice-versa (Miao et al., 2018; Zheng et al., 2017). Therefore,  $PM_{2.5}$  usually  
148 has an anticorrelation with BLH. However, for wildfire events, the aerosol layer height is  
149 sometimes higher than the BLH (Haarig et al., 2018), which leads to lower correlation between  
150 AOD and  $PM_{2.5}$  since we use only BLH to present the aerosol layer height. Thus BLH can provide  
151 aerosol vertical information in most cases except for suspended high-layer aerosol caused by fires,  
152 which leads to higher bias of the model for high-layer aerosols near the fire sources. Surface  
153 temperature (T2M) can affect  $PM_{2.5}$  through convection, evaporation, temperature inversion and  
154 secondary pollutants generation processes (Chen et al., 2020). The first two processes are  
155 negatively related to  $PM_{2.5}$  concentration: 1) higher temperature increases turbulence and  
156 atmospheric convections which accelerate the pollution dispersion ( $PM_{2.5}$  decreases); 2) higher  
157 temperature increases evaporation loss of  $PM_{2.5}$  including ammonium nitrate and other volatile or

158 semi-volatile components (Wang et al., 2017). The later two processes are positively related to  $PM_{2.5}$   
159 by limiting vertical motion and promoting photochemical reactions under high temperature (Xu et  
160 al., 2019; Zhang et al., 2015). Wind speed (WS) are often negatively related to  $PM_{2.5}$  since it  
161 increases the dispersion of pollutants. However, unique geographical conditions (such like  
162 mountains) with certain wind directions can cause accumulations of pollutants (Chen et al., 2017).  
163 RH may promote hygroscopic growth of particles to increase  $PM_{2.5}$  (Trueblood et al., 2018; Zheng  
164 et al., 2017), but it can also reduce  $PM_{2.5}$  through the deposition process. SP may influence the  
165 diffusion or accumulation of pollutants through formation of low-level wind convergence (You et  
166 al., 2017).

Formatted: Font:

### 167 3. Methodology

168 To assess the impact of NWUSC fires on  $PM_{2.5}$  in the United States, we first estimate the  
169  $PM_{2.5}$  over the study region during a time period with high fire activity (2018). We then use the  
170 same method during a year with low fire activity (2011) to compare the differences between the  
171 two years. The two years are selected based on the total FRP in August calculated within Canada  
172 ( $49^{\circ}\sim 60^{\circ}\text{N}$ ,  $55^{\circ}\sim 135^{\circ}\text{W}$ ) and Northwestern (NW) US ( $35^{\circ}\sim 49^{\circ}\text{N}$ ,  $105^{\circ}\sim 125^{\circ}\text{W}$ ). Table 2 shows the  
173 total FRP in Canada and Northwestern US in August from 2010 to 2018. The total FRP in the two  
174 regions is lowest in 2011 and highest in 2018 during the 9 years, which provides the basis for the  
175 study. In order to create a  $0.1^{\circ}$  surface  $PM_{2.5}$ , the GWR model is used to estimate the relationships  
176 of  $PM_{2.5}$  and AOD. Detailed processing steps for GWR model are shown in Figure 1.

177 **3.1 Data preprocessing:** The first step is to resample all datasets to a uniform spatial resolution  
178 by creating a  $0.1^{\circ}$  resolution grid covering the Continental United States. During this process, we  
179 collocate the  $PM_{2.5}$  data and average the values if there is more than one value in one grid. Then



180 the MAIAC AOD and smoke flagare averaged into  $0.1^\circ$  grid cells. Meteorological datasets are  
181 also resampled to the  $0.1^\circ$  grid cells by applying the inverse distance method.

182 **3.2 Time selecting & averaging:** Next we select data where AOD and ground  $PM_{2.5}$  are both  
183 available ( $AOD > 0$  and  $PM_{2.5} > 2.0 \mu g m^{-3}$ ) and average them for the study period. This is to  
184 ensure that the AOD,  $PM_{2.5}$  and other variables match with each other, because  $PM_{2.5}$  is not a  
185 continuous measurement for some sites and AOD have missing values due to cloud cover and  
186 other reasons. Therefore, it is important to use data from days where both measurements are  
187 available to avoid sampling biases.

188 **3.3 GWR model development and validation:** The Adaptive bandwidth selected by the Akaike's  
189 Information Criterion (AIC) is used for the GWR model (Loader, 1999). For locations that already  
190 have  $PM_{2.5}$  monitors, we calculate the mean AOD of a  $0.5 \times 0.5^\circ$  box centered at the ground location  
191 and estimate the GWR coefficients ( $\beta$ ) for AOD and meteorological variables to estimate  $PM_{2.5}$ .  
192 The model structure can be expressed as:

$$193 \quad PM_{2.5i} = \beta_{0,i} + \beta_{1,i}AOD_i + \beta_{2,i}BLH_i + \beta_{3,i}T2M_i + \beta_{4,i}U10M_i + \beta_{5,i}RH_{sfc_i} + \beta_{6,i}SP_i + \beta_{7,i}SF_i \\ 194 \quad \quad \quad + \varepsilon_i$$

195 where  $PM_{2.5i}$  ( $\mu g m^{-3}$ ) is the selected ground-level  $PM_{2.5}$  concentration at location  $i$ ;  $\beta_{0,i}$   
196 is the intercept at location  $i$ ;  $\beta_{1,i} \sim \beta_{8,i}$  are the location-specific coefficients;  $AOD_i$  is the resampled  
197 AOD selected from MAIAC daily AOD data at location  $i$ ;  $BLH_i, T2M_i, U10M_i, RH_{sfc_i}, SP_i$  are  
198 selected meteorological parameters (BLH, T2M, WS, RH and PS) at location  $i$ ;  $SF_i$  (%) is the  
199 resampled smoke flag data at location  $i$  and  $\varepsilon_i$  is the error term at location  $i$ .

200 We perform the Leave One Out Cross Validation (LOOCV) to test the model predictive  
201 performance (Kearns and Ron, 1999). Since the GWR model relies on adequate number of

202 observations, the prediction accuracy will be lower if we preserve too much data for validation.  
203 Therefore, we choose the LOOCV method, which preserve only one data for validation at a time  
204 and repeat the process until all the data are used. In addition,  $R^2$  and RMSE are calculated for both  
205 model fitting and model validation process to detect overfitting. Model overfitting will lead to low  
206 predictability, which means it fits too close to the limited number of data to predict for other places  
207 and will cause large bias.

208 **3.4 Model prediction:** While predicting the ground-level  $PM_{2.5}$  for unsampled locations, we make  
209 use of the estimated parameters for sites within a  $5^\circ$  radius to generate new slopes for independent  
210 variables based on the spatial weighting matrix (Brunsdon et al., 1996). The closer to the predicted  
211 location, the closer to 1 the weighting factor will be, while the weighting factor for sites further  
212 than the  $5^\circ$  in distance is zero. It is important to note that AOD and other independent variables  
213 used for prediction in this step are averaged values for days that have valid AOD, which is different  
214 from the data used in the fitting process since  $PM_{2.5}$  is not measured every day in all locations.

## 215 **4. Results and Discussion**

216 We first discuss the surface  $PM_{2.5}$  for a few select locations that are impacted by fires  
217 followed by the spatial distribution of MODIS AOD and the FRP for August 2018. We then assess  
218 the spatial distribution of surface  $PM_{2.5}$  from the GWR method. The validation of the GWR method  
219 is then discussed. To further demonstrate the impact of the NWUSC fires on  $PM_{2.5}$  air quality in  
220 the United States, we show the spatial distribution of the difference between August 2018 and  
221 August 2011. We further quantify these results for ten US EPA regions.

### 222 **4.1 Descriptive statistics of satellite data and ground measurements**

223           The 2018 summertime Canadian wildfires started around the end of July in British  
224 Columbia and continued until mid-September. The fires spread rapidly to the south of Canada  
225 during August, causing high concentrations of smoke aerosols to drift down to the US and affecting  
226 particulate matter air quality significantly. From late July to mid-September, wildfires in the  
227 northwest US that burnt forest and grassland also affected air quality. Starting with the Cougar  
228 Creek Fire, then Crescent Mountain and Gilbert Fires, different wildfires in in NWUSC caused  
229 severe air pollution in various US cities. Figure 2a shows the rapid increase in  $PM_{2.5}$  of selected  
230 US cities from July 1<sup>st</sup> to August 31<sup>st</sup>, due to the transport of smoke from these wildfires. For all  
231 sites, July had low  $PM_{2.5}$  concentrations ( $<10 \mu g m^{-3}$ ) and rapidly increases as fire activity  
232 increases. Calculating only from the EPA ground observations, the mean  $PM_{2.5}$  of the 17 days for  
233 the whole US is  $13.7 \mu g m^{-3}$  and the mean  $PM_{2.5}$  for Washington (WA) is  $40.6 \mu g m^{-3}$ , which  
234 indicates that the PM pollution is concentrated in the northwestern US for these days. This trend  
235 is obvious when comparing the mean  $PM_{2.5}$  of all US stations (black line with no markers) and the  
236 mean  $PM_{2.5}$  of all WA stations (grey line with no markers). Ground-level  $PM_{2.5}$  reaches its peak  
237 between August 17<sup>th</sup>-21<sup>st</sup> and daily  $PM_{2.5}$  values during this time period far exceeds the 17-day  
238 mean  $PM_{2.5}$ . For example, mean  $PM_{2.5}$  in WA on August 20<sup>th</sup> is  $86.75 \mu g m^{-3}$ , which is more  
239 than two times the 17-day average of this region. On August 19<sup>th</sup>, Omak which is located in the  
240 foothills of the Okanogan Highlands in WA had  $PM_{2.5}$  values exceed  $250 \mu g m^{-3}$ . According to  
241 a review of US wildfire caused  $PM_{2.5}$  exposures, 24-h mean  $PM_{2.5}$  concentrations from wildfires  
242 ranged from 8.7 to  $121 \mu g m^{-3}$ , with a 24 h maximum concentration of  $1659 \mu g m^{-3}$  (Navarro et  
243 al., 2018).

244           Table 3 shows relevant statistics of 15 states that have at least one daily record of non-  
245 attainment of EPA standard ( $>35 \mu g m^{-3}$ ). From the frequency records of non attainment in the

246 17-day period (last column), four states (Montana, Washington, California and Idaho) were  
247 consistently affected by the wildfires, and large portion of ground stations in these states were  
248 influenced by smoke aerosols. Most of the neighboring states also suffered from short-term but  
249 broad air pollution (third column). Noticeable from these records is that the total number of ground  
250 stations in some of the highly affected states (such as Idaho) is not sufficient for capturing the  
251 smoke. Although there are total 8 EPA stations in Idaho, only two of them have consistent  
252 observations during the fire event; the other two stations have no valid observations, and the  
253 remaining four stations have only 2~6 observations during the 17-day period. Limited valid data  
254 along with unevenly distributed stations makes it hard to quantify smoke pollution in Northwestern  
255 US during the fire event period. Therefore, we utilize satellite data to enlarge the spatial coverage  
256 and estimate pollution at a finer spatial resolution.

257 The spatial distribution of AOD shown in Figure 2b indicates that the smoke from Canada  
258 is concentrated mostly in Northern US states such as WA, Oregon, Idaho, Montana, North Dakota  
259 and Minnesota. The black arrow shows the mean 800hPa-level mean wind for 17 days, and the  
260 length of the arrow represents the wind speed in  $\text{ms}^{-1}$ . Also shown in Figure 2b are wind speeds  
261 close to the fire sources which are about  $4\sim 5 \text{ ms}^{-1}$ , and according to the distances and wind  
262 directions, it can take approximately 28~36 hours for the smoke to transport southeastward to  
263 Washington state. Then the smoke continues to move east to other northern states such as Montana  
264 and North Dakota. In addition, the grey circle represents the total fire radiative power (FRP) of  
265 every  $2.3\times 3.5$ -degree box. The reason for not choosing a smaller grid for the FRP is to not clutter  
266 Figure 2b with information from small fires. The bigger the circle is, the stronger the fire is in that  
267 grid and different sizes and its corresponding FRP values are shown in the lower right corner. It is  
268 clear that the strongest fires in 2018 are located in the Tweedsmuir Provincial Park of British

269 Columbia in Canada (53.333N, 126.417W). The four separate lightning-caused wildfires burnt  
270 nearly 301,549 hectares of the boreal forest. The total FRP of August 2018 in Canada is about  
271 5362 (\*1000 MW), while the total FRP of August 2011 in Canada is 48 (\* 1000 MW). The 2011  
272 fire was relatively weak compared to the 2018 Tweedsmuir Complex fire and we therefore use the  
273 2011 air quality data as a baseline to quantify the 2018 fire influence on  $PM_{2.5}$  in the United States.

#### 274 **4.2 Model Fitting and validation**

275 The main goal for using GWR model is to help predict the spatial distribution of  $PM_{2.5}$  for  
276 places with no ground monitors while leveraging the satellite AOD and therefore it is important to  
277 ensure that the model is robust. Figure 3a and 3b show the results for 2018 for GWR model fitting  
278 for the entire US and the LOOCV models respectively. The color of the scatter plots represents  
279 the probability density function (PDF) which calculates the relative likelihood that the observed  
280 ground-level  $PM_{2.5}$  would equal the predicted value. The lighter the color is, the more points are  
281 present, with a higher correlation. The model fitting process estimates the slope for each variable  
282 and therefore the model can be fitted close to the observed  $PM_{2.5}$  and using this estimated  
283 relationship we are able to assess surface  $PM_{2.5}$  using other parameters at locations where  $PM_{2.5}$   
284 monitors are not available. The LOOCV process tests the model performance in predicting  $PM_{2.5}$ .  
285 If the results of LOOCV has a large bias from the model fitting, then the predictability of the model  
286 is low. Higher  $R^2$  difference and RMSE difference value indicate that the model is overfitting and  
287 not suitable. The  $R^2$  for the model fitting is 0.834, and the  $R^2$  for the LOOCV is 0.797; the RMSE  
288 for the GWR model fitting is  $3.46 \mu g m^{-3}$ , and for LOOCV the RMSE is  $3.84 \mu g m^{-3}$ . There are  
289 minor differences between fitting  $R^2$  and validation  $R^2$  (0.037) and between fitting RMSE and  
290 validation RMSE ( $0.376 \mu g m^{-3}$ ) suggesting that the model is not over-fitting and has stable  
291 predictability further indicating that the model can predict surface  $PM_{2.5}$  reliably. In addition, we

292 also performed a 20-fold cross validation by splitting the dataset into 20 consecutive folds, and  
293 each fold is used for validation while the 19 remaining folds form the training set. The 20-fold  
294 cross validation has  $R^2$  of 0.745 and RMSE of  $4.3 \mu g m^{-3}$ . The increase/decrease in the cross  
295 validated  $R^2$  and RMSE indicates the importance of sufficient data used for fitting since a small  
296 decrease in the number of fitting data can reduce the model prediction accuracy. Overall, the  
297 prediction error of the model is between  $3\sim 5 \mu g m^{-3}$ , which is a reasonable error range for 17-day  
298 average prediction of  $PM_{2.5}$ . For data greater than the EPA standard ( $35 \mu g m^{-3}$ ), the model has  
299 a RMSE of  $12.07 \mu g m^{-3}$ , which is a lot larger than the RMSE when using the entire model.  
300 Therefore, the model has a tendency for underestimating  $PM_{2.5}$  exceedances by around  $12.07$   
301  $\mu g m^{-3}$ . The larger the  $PM_{2.5}$  is, the greater the model underestimates. To examine the model  
302 performance for high and low polluted areas, the results are divided into two parts (larger than  $35$   
303  $\mu g m^{-3}$  and less than  $35 \mu g m^{-3}$ ). Areas with high pollution have  $R^2$  of 0.64 and areas with low  
304 pollution have  $R^2$  of 0.67, therefore, the model performance is relative stable for both large and  
305 small  $PM_{2.5}$  values. Also, the inclusion of low aerosol concentration areas does not influence the  
306 model performance for high values (seen in supplemental material in Figures S1 and S2), which  
307 means that the high  $R^2$  is not a reason of large number of low values.

#### 308 4.3 Predictors' influence during wildfires

309 Table 4 shows the GWR model mean coefficients for the whole US region and for different  
310 selected regions. The selected boxes are shown in figure 4c in different colors: box1 (red) located  
311 in NW US include major fire sources in US; box2 (gold) located in Montana state is influenced  
312 from both neighboring states and smoke from Canada; box3 (green) in Minnesota which is located  
313 further from the fires and has minor increase in  $PM_{2.5}$  due to remote smoke; box4 (black) in NE  
314 (Northeast) US is the furthest from fires and has no obvious pollution increase. The second column

315 of the tables shows the conditions for sample selection and the third column shows the number of  
316 pixels selected for each box. By comparing the coefficients of samples selected in these boxes,  
317 predictors have different influence in different locations. AOD has stronger influence on predicting  
318  $PM_{2.5}$  closer to fire sources, but local emissions become more dominant if the distances is large  
319 enough. The smoke flag is overall positive related to surface  $PM_{2.5}$ , while it could slightly  
320 negatively relate to  $PM_{2.5}$  around fire sources and northeastern coasts. PBL is negatively related to  
321  $PM_{2.5}$  when the pollution is concentrated near the surface (fires or human-made emissions), while  
322 it appears to be positively related to  $PM_{2.5}$  at locations where the main pollution source comes  
323 from remote wildfire smoke. Surface temperature have a relative stable positive correlation with  
324 surface  $PM_{2.5}$ , however, surface pressure and wind speeds are negatively correlated with  $PM_{2.5}$ .  
325 Relative humidity, on the other hand, shows large variations on  $PM_{2.5}$  influence across the nation.  
326 Around the wildfires where the RH is relative low, RH has a positive correlation with  $PM_{2.5}$  since  
327 hygroscopicity would increase and leads to accumulation of  $PM_{2.5}$ , but increasing RH can also  
328 decrease  $PM_{2.5}$  concentration by overgrowing the  $PM_{2.5}$  particles to deposition at high RH  
329 environment (Chen et al., 2018).

330 From table 4, we know that the weighting for AOD is much larger than other predictors, but  
331 predictors other than AOD are important for the prediction. We tested our model with AOD as the only  
332 predictor to conduct a comparison with the original model, and the  $R^2$  decreases from 0.83 to 0.79 and  
333 RMSE increases from 3.46 to 3.8. This is consistent with previous study (Jiang et al., 2017) which  
334 shows improvements of  $R^2$  from 0.69 to 0.78 and RMSE from 7.25 to 6.18 by adding 4 meteorological  
335 parameters in summer in easter China. Other predictors have higher weighting at the fire source region  
336 (box1) where BLH cannot provide the aerosol vertical distribution information since smoke tends to  
337 be injected to higher levels. For high AOD regions where aerosol tends to be suspended at high levels,  
338 adding other predictors other than AOD tends to have lower improvement of the model compared with

Formatted: Default, Space After: 8 pt

339 low AOD values, because adding BLH can significantly improve the prediction for low level aerosols.  
340 For regions with AOD less than 35,  $R^2$  increases 0.09 from AOD only model (0.6 to 0.69), while  $R^2$   
341 increases 0.05 for areas with AOD larger than 35. RMSE decreases 12% and 7% for AOD less and  
342 larger than 35 conditions, respectively. Overall, the meteorological factors have larger improvements  
343 for low polluted areas (low level aerosol in this case).

Formatted: Font: 11.5 pt, Font color: Text 1

#### 344 **4.4 Predicted PM<sub>2.5</sub> Distribution**

345 The mean PM<sub>2.5</sub> distributions over the United States shown in Figure 4a is calculated by  
346 averaging the surface PM<sub>2.5</sub> data from ground monitors for the 17 days, which matches well with  
347 the GWR model-predicted PM<sub>2.5</sub> distributions shown in Figure 4b. The model estimation extends  
348 the ground measurements and provide pollution assessments across the entire nation. Comparing  
349 the AOD map (Figure 2b) with the PM<sub>2.5</sub> estimations (Figure 4b), demonstrates the differences  
350 between columnar and surface-level pollution. Differences between the AOD and PM<sub>2.5</sub>  
351 distributions are due to various reasons including 1) Areas with high PM<sub>2.5</sub> concentrations in figure  
352 4b correspond to low AOD values in figure 2b (Southern California, Utah, and southern US); 2)  
353 and high AOD regions in figure 2b correspond to low PM<sub>2.5</sub> concentrations in figure 4b  
354 (Minnesota). The first situation usually occurs at the edge of polluted areas that are relative far  
355 from the fire source, which is consistent with previous studies that reported smaller particles (<10  
356  $\mu g$ ) are able to travel longer distances compared to large particles (>10  $\mu g$ ) (Gillies et al., 1996),  
357 and that larger particles tend to settle closer to their source (Sapkota et al., 2005; Zhu et al., 2002).

358 We use the same method for August 9<sup>th</sup> to August 25<sup>th</sup> in 2011 that had low fire activity,  
359 ensuring consistency for estimating coefficients for different variables for 2011. Figure 4c shows  
360 the difference in spatial distribution of mean ground PM<sub>2.5</sub> of the 17 days between 2018 and 2011.  
361 High values of PM<sub>2.5</sub> differences are in the Northwestern and central parts of the United States



362 with the Southern states having very little impact due to the fires. Of all the 48 states within the  
363 study region, there are 29 states that have a higher PM<sub>2.5</sub> value in 2018 than 2011, and 15 states  
364 have 2018 PM<sub>2.5</sub> value more than two times their 2011 value (shown in figure 5). The mean PM<sub>2.5</sub>  
365 for WA increases from 5.87 in 2011 to 46.47  $\mu\text{g m}^{-3}$  in 2018, which is about 8 times more than  
366 2011 values. The PM<sub>2.5</sub> values in Oregon increases from 4.97 (in 2011) to 33.3  $\mu\text{g m}^{-3}$  in 2018,  
367 which is nearly seven times more than in 2011. For states from Montana to Minnesota, the mean  
368 PM<sub>2.5</sub> decreases from east to west, which reveals the path of smoke transport. As shown in Figure  
369 4c, there is a clear transport path of smoke from North Dakota all the way to Texas. Along the  
370 path, smoke increases PM<sub>2.5</sub> concentrations by 168% in North Dakota and 27% in Texas. Smoke  
371 aerosols transported over long distances contains fine fraction PM which significantly affect the  
372 health of children, adults, and vulnerable groups.

373 Figure 5 shows the mean PM<sub>2.5</sub> predicted from the GWR model of different EPA regions  
374 for the 17 days in 2011 and 2018 (Hawaii and Alaska are not included). The most influenced region  
375 is region 10, which has a 2018 mean PM<sub>2.5</sub> value of 34.2  $\mu\text{g m}^{-3}$  that is 6 times larger than the  
376 values in 2011 (5.8  $\mu\text{g m}^{-3}$ ) values. The PM<sub>2.5</sub> of region 8 and 9 have 2.4 and 2.6 times increase  
377 in 2018 compared to 2011. Region 1~4 have lower PM<sub>2.5</sub> in 2018 than 2011 possibly due to Clean  
378 Air Act initiatives, absence of any major fire activities and further away for transported aerosols.  
379 The emission reduction improves the US air quality and lower the PM<sub>2.5</sub> every year, but 6 out of  
380 10 EPA regions show significant increases in PM<sub>2.5</sub> during the study period, which indicates that  
381 the long-range transported wildfire smoke has become the new major pollutant in the US.

#### 382 **4.5 Estimation of Canadian fire pollution**

383 To evaluate the pollution caused only from Canadian fires, we did a rough assessment  
384 according to the total FRP and PM<sub>2.5</sub> values. There are three states in the US have wildfires during

385 the study period: California, Washington and Oregon, and they have total FRP of 1186, 518 and  
386 439 (\*1000 MW) respectively. Assuming that California was only influenced by the local fires,  
387 then fires of 1186 (\*1000 MW) cause  $13 \mu\text{g m}^{-3}$  increase in  $\text{PM}_{2.5}$ . Accordingly, wildfires in  
388 Washington and Oregon State will cause 6 and  $5 \mu\text{g m}^{-3}$  increase in state mean  $\text{PM}_{2.5}$ . Therefore,  
389 Canadian fires caused  $\text{PM}_{2.5}$  increase in Washington and Oregon is about 35 and  $23 \mu\text{g m}^{-3}$ . Since  
390 the FRP of Canadian wildfires are approximately 5 times larger than that of the California fires,  
391 which is the strongest fire in US, we assume the pollution affecting the states located in the  
392 downwind directions other than the three states are mainly coming from Canadian wildfires. States  
393 with no local fires such as Montana, North Dakota, South Dakota and Minnesota have  $\text{PM}_{2.5}$   
394 increase of 18.31, 12.8, 10.4 and  $10.13 \mu\text{g m}^{-3}$ . The decrease of these numbers reveal that the  
395 smoke is transport in a SE direction. This influence of Canadian wildfires on US air quality is only  
396 a rough quantity estimation, thus additional work is needed for understand long-range transport  
397 smoke pollution and its impact on public health. One way to do this would be assessing the  
398 difference of pollution by turning on and off US fires in chemistry models.

#### 399 4.6 eComparison with previous studies

400 Comparing with the Bayesian ensemble model developed by Geng et al. (Geng et al., 2018)  
401 using MAIAC AOD and CMAQ (Community Multiscale Air Quality) model and ground  $\text{PM}_{2.5}$   
402 measurements, our GWR model has larger  $R^2$ , but with the chemistry transport model (CTM),  
403 their method can provide more vertical distribution information which is important for wildfire  
404 smoke. GWR usually have better accuracy than CTM since there are large uncertainties related to  
405 different CTM inputs such as emission, meteorological and land cover data, but for regions with  
406 less or no ground measurements, CTM provide a great approach for estimating surface  $\text{PM}_{2.5}$ .  
407 Other studies which used machine learning method to predict surface  $\text{PM}_{2.5}$  have better

Formatted: Font: Bold

Formatted: Font: Bold

408 performance for long-term prediction rather than monthly estimation (Liang et al., 2020; Xiao et  
409 al., 2018), but can better resolve complex relationship between different predictors than statistical  
410 models (Geng et al., 2020). For wildfire events, the available data is much less than the long-term  
411 aerosol analysis, so the performance of machine learning method could be less accurate compared  
412 to long-term prediction. Our study also shows slightly larger  $R^2$  compared to other GWR studies  
413 (Hu et al., 2013; Ma et al., 2014; You et al., 2016) due to the inclusion of more meteorological and  
414 other related predictors.

Formatted: Font:

#### 415 **4.7.6 Model uncertainties and limitations**

416 There are various sources of uncertainties and limitations for studies that use satellite data  
417 to estimate surface  $PM_{2.5}$  concentrations. Since wildfires develop quickly it is important to have  
418 continuous observations to capture the rapid changes. This study uses polar orbiting high-quality  
419 satellite aerosol products, but the temporal evolution can only be estimated by geostationary data  
420 sets. Although satellite observations have excellent spatial coverage, missing data due to cloud  
421 cover is a limitation. As discussed in the paper, the prediction error (RMSE) of the model is  
422 between  $3\text{--}5 \mu\text{g m}^{-3}$ , while the RMSE increased for locations with high aerosol concentration.  
423 This is partly due to lack of accurate vertical distribution information which is very important for  
424 wildfire smoke. The GWR model is largely influenced by the distribution of ground stations, and  
425 the prediction error will be different in different places due to unevenly distributed  $PM_{2.5}$  stations.  
426 For locations that have a dense ground-monitoring distribution, the prediction error will be low,  
427 while the prediction error will be relative larger at other places with sparse surface stations.  
428 Although there are obvious limitations, complementing surface data with satellite products and  
429 meteorological and other ancillary information in a statistical model like the GWR has provided  
430 robust results for estimating surface  $PM_{2.5}$  from wildfires. We also note that we did not consider

431 some variables used in other studies such as NDVI, forest cover, vegetation type, industrial  
432 density, visibility and chemical constituents of smoke particles (Donkelaar et al., 2015; Hu et al.,  
433 2013; You et al., 2015; Zou et al., 2016). Visibility mentioned in some studies may improve the  
434 model performance, but unlike AOD, it has limited measurement across the nation, which will  
435 restrict the applicability of training data. Another uncertainty comes from the 2011 wildfires which  
436 we assumed to be zero fire events but there are actually few fire events in EPA region 6, 8, 9 and  
437 10, and this will lead to underestimation of  $PM_{2.5}$  increase due to 2018 fires in these regions.

438 One limitation of this study is that analysis based on 17-day mean values cannot capture  
439 daily pollution variations, which is also very important for pollution estimation during rapid-  
440 changing wildfire events. To extend this analysis to daily estimation, the cloud contaminations of  
441 satellite observations become a major problem. Therefore, future work is needed using chemistry  
442 transport models and other data to fill in the gaps on missing AOD data due to cloud coverage.

## 443 **5. Summary and Conclusions**

444 We estimate the surface mean  $PM_{2.5}$  for 17 days in August for a high fire active year (2018)  
445 and compare that with a low fire activity year using the Geographically Weighted Regression  
446 (GWR) method to assess the increase in  $PM_{2.5}$  in the United States due to smoke transported from  
447 fires. The difference in  $PM_{2.5}$  between the two years indicates that more than half of the US states  
448 (29 states) are influenced by the NWUSC wildfires, and half of the affected states have 17-day  
449 mean  $PM_{2.5}$  increases larger than 100% of the baseline value. The peak  $PM_{2.5}$  during the wildfires  
450 can be much larger than the 17-day average and can affect vulnerable populations susceptible to  
451 air pollution. Some of the most affected states are in Washington, California, Wisconsin, Colorado  
452 and Oregon, all of which have populations greater than 4 million. According to CDC (Centers for  
453 Disease Control and Prevention), 8% of the population have asthma (CDC, 2011). Therefore, for

Xue, Gupta, Christopher, submitted to Atmospheric Chemistry and Physics

454 asthma alone, there are about 3 million people facing significant health issue due to the long-range  
455 transport smoke in these states.

456 For states that show decrease in PM<sub>2.5</sub> due to the Clean Air Act, the mean decrease is about  
457 16% of the baseline after 7 years. This is consistent with EPA's report that there is a 23% decrease  
458 of PM<sub>2.5</sub> in national average from 2010 to 2019(U.S. Environmental Protection Agency, 2019).  
459 Comparing with the dramatic increase (132%) caused by wildfires, pollution from the fires is  
460 counteracting our effort on emission controls. Although wildfires are often episodic and short-  
461 term, high frequency of fire occurrence and increasing longer durations of summertime wildfires  
462 in recent years has made them now a long-term influence on public lives. Our results show a  
463 significant increase of pollution in a short time period in most of the US states due to the NWUSC  
464 wildfires, which affects millions of people. With wildfires becoming more frequent during recent  
465 years, more effort is needed to predict and warn the public about the long-range transported smoke  
466 from wildfires.

#### 467 **Acknowledgements.**

468 Pawan Gupta was supported by a NASA Grant. MODIS data were acquired from the Goddard  
469 DAAC. We Sincerest thanks to the MAIAC, MODIS, EPA and ECMWF teams for their datasets  
470 that makes all the data providers for making this research possible.

#### 471 **References**

472 Apte, J.S., Brauer, M., Cohen, A.J., Ezzati, M., Pope, C.A., 2018. Ambient PM<sub>2.5</sub> Reduces

473 Global and Regional Life Expectancy. Environ. Sci. Technol. Lett. 5, 546–551.

474 <https://doi.org/10.1021/acs.estlett.8b00360>

475 Brunson, C., Fotheringham, A.S., Charlton, M.E., 1996. Geographically Weighted Regression:

Xue, Gupta, Christopher, submitted to Atmospheric Chemistry and Physics

- 476 A Method for Exploring Spatial Nonstationarity. *Geogr. Anal.* 28, 281–298.  
477 <https://doi.org/https://doi.org/10.1111/j.1538-4632.1996.tb00936.x>
- 478 Calkin, D.E., Thompson, M.P., Finney, M.A., 2015. Negative consequences of positive  
479 feedbacks in us wildfire management. *For. Ecosyst.* 2, 1–10.  
480 <https://doi.org/10.1186/s40663-015-0033-8>
- 481 Cascio, W.E., 2018. Wildland Fire Smoke and Human Health. *Sci. Total Environ.* 624, 586–595.  
482 <https://doi.org/10.1016/j.scitotenv.2017.12.086>.
- 483 CDC, 2011. Asthma in the US. *CDC Vital Signs* 1–4.
- 484 Chen, D., Xie, X., Zhou, Y., Lang, J., Xu, T., Yang, N., Zhao, Y., Liu, X., 2017. Performance  
485 evaluation of the WRF-chem model with different physical parameterization schemes  
486 during an extremely high PM<sub>2.5</sub> pollution episode in Beijing. *Aerosol Air Qual. Res.* 17,  
487 262–277. <https://doi.org/10.4209/aaqr.2015.10.0610>
- 488 Chen, Z., Chen, D., Zhao, C., Kwan, M. po, Cai, J., Zhuang, Y., Zhao, B., Wang, X., Chen, B.,  
489 Yang, J., Li, R., He, B., Gao, B., Wang, K., Xu, B., 2020. Influence of meteorological  
490 conditions on PM<sub>2.5</sub> concentrations across China: A review of methodology and  
491 mechanism. *Environ. Int.* 139, 105558. <https://doi.org/10.1016/j.envint.2020.105558>
- 492 Chen, Z., Xie, X., Cai, J., Chen, D., Gao, B., He, B., Cheng, N., Xu, B., 2018. Understanding  
493 meteorological influences on PM<sub>2.5</sub> concentrations across China: A temporal and spatial  
494 perspective. *Atmos. Chem. Phys.* 18, 5343–5358. <https://doi.org/10.5194/acp-18-5343-2018>
- 495 Chu, Y., Liu, Y., Li, X., Liu, Z., Lu, H., Lu, Y., Mao, Z., Chen, X., Li, N., Ren, M., Liu, F., Tian,  
496 L., Zhu, Z., Xiang, H., 2016. A review on predicting ground PM<sub>2.5</sub> concentration using

Xue, Gupta, Christopher, submitted to Atmospheric Chemistry and Physics

- 497 satellite aerosol optical depth. *Atmosphere (Basel)*. 7, 129.  
498 <https://doi.org/10.3390/atmos7100129>
- 499 Coogan, S.C.P., Robinne, F.N., Jain, P., Flannigan, M.D., 2019. Scientists' warning on wildfire  
500 — a canadian perspective. *Can. J. For. Res.* 49, 1015–1023. [https://doi.org/10.1139/cjfr-](https://doi.org/10.1139/cjfr-2019-0094)  
501 2019-0094
- 502 Donkelaar, A. Van, Martin, R. V., Li, C., Burnett, R.T., 2019. Regional Estimates of Chemical  
503 Composition of Fine Particulate Matter Using a Combined Geoscience-Statistical Method  
504 with Information from Satellites, Models, and Monitors. *Environ. Sci. Technol.* 53, 2595–  
505 2611. <https://doi.org/10.1021/acs.est.8b06392>
- 506 Donkelaar, A. Van, Martin, R. V., Park, R.J., 2006. Estimating ground-level PM<sub>2.5</sub> using  
507 aerosol optical depth determined from satellite remote sensing. *J. Geophys. Res. Atmos.*  
508 111. <https://doi.org/10.1029/2005JD006996>
- 509 Donkelaar, A. Van, Martin, R. V., Spurr, R.J.D., Burnett, R.T., 2015. High-Resolution Satellite-  
510 Derived PM<sub>2.5</sub> from Optimal Estimation and Geographically Weighted Regression over  
511 North America. *Environ. Sci. Technol.* 49, 10482–10491.  
512 <https://doi.org/10.1021/acs.est.5b02076>
- 513 Dreessen, J., Sullivan, J., Delgado, R., 2016. Observations and impacts of transported Canadian  
514 wildfire smoke on ozone and aerosol air quality in the Maryland region on June 9–12, 2015.  
515 *J. Air Waste Manag. Assoc.* 66, 842–862. <https://doi.org/10.1080/10962247.2016.1161674>
- 516 Fotheringham, A.S., Charlton, M.E., Brunson, C., 1998. Geographically weighted regression: a  
517 natural evolution of the expansion method for spatial data analysis. *Environ. Plan. A* 30,  
518 1905–1927.

Xue, Gupta, Christopher, submitted to Atmospheric Chemistry and Physics

- 519 Fotheringham, S.A., Brunson, C., Charlton, M., 2003. Geographically Weighted Regression :  
520 The Analysis of Spatially Varying Relationships, John Wiley and Sons.
- 521 Freeborn, P.H., Wooster, M.J., Roy, D.P., Cochrane, M.A., 2014. Quantification of MODIS fire  
522 radiative power (FRP) measurement uncertainty for use in satellite-based active fire  
523 characterization and biomass burning estimation. *Geophys. Res. Lett.* 41, 1988–1994.  
524 <https://doi.org/10.1002/2013GL059086>.
- 525 Goldberg, D.L., Gupta, P., Wang, K., Jena, C., Zhang, Y., Lu, Z., Streets, D.G., 2019. Using gap-  
526 filled MAIAC AOD and WRF-Chem to estimate daily PM<sub>2.5</sub> concentrations at 1 km  
527 resolution in the Eastern United States. *Atmos. Environ.* 199, 443–452.  
528 <https://doi.org/10.1016/j.atmosenv.2018.11.049>
- 529 Gu, Y., 2019. Estimating PM<sub>2.5</sub> Concentrations Using 3 km MODIS AOD Products : A Case  
530 Study in British Columbia , Canada. University of Waterloo.
- 531 Guo, B., Wang, X., Pei, L., Su, Y., Zhang, D., Wang, Y., 2021. Identifying the spatiotemporal  
532 dynamic of PM<sub>2.5</sub> concentrations at multiple scales using geographically and temporally  
533 weighted regression model across China during 2015–2018. *Sci. Total Environ.* 751.  
534 <https://doi.org/10.1016/j.scitotenv.2020.141765>
- 535 Gupta, P., Christopher, S.A., 2009a. Particulate matter air quality assessment using integrated  
536 surface, satellite, and meteorological products: 2. A neural network approach. *J. Geophys.*  
537 *Res. Atmos.* 114, 1–14. <https://doi.org/10.1029/2008JD011497>
- 538 Gupta, P., Christopher, S.A., 2009b. Particulate matter air quality assessment using integrated  
539 surface , satellite , and meteorological products : Multiple regression approach. *J. Geophys.*  
540 *Res. Atmos.* 114, 1–13. <https://doi.org/10.1029/2008JD011496>



- 541 Haarig, M., Ansmann, A., Baars, H., Jimenez, C., Veselovskii, I., Engelmann, R., Althausen, D.,  
542 2018. Extreme levels of Canadian wildfire smoke in the stratosphere over central Europe –  
543 Part 2: Lidar study of depolarization and lidar ratios at 355, 532, and 1064 nm and of  
544 microphysical properties. *Atmos. Chem. Phys. Discuss.* 1–22. [https://doi.org/10.5194/acp-](https://doi.org/10.5194/acp-2018-358)  
545 2018-358
- 546 Hall, E.S., Kaushik, S.M., Vanderpool, R.W., Duvall, R.M., Beaver, M.R., Long, R.W.,  
547 Solomon, P.A., 2013. Integrating Sensor Monitoring Technology into Current Air  
548 Pollution Regulatory Support Paradigm: Practical Considerations. *Am. J. Environ. Eng* 4,  
549 147–154. <https://doi.org/10.5923/j.ajee.20140406.02>
- 550 Hessburg, P.F., Churchill, D.J., Larson, A.J., Haugo, R.D., Miller, C., Spies, T.A., North, M.P.,  
551 Povak, N.A., Belote, R.T., Singleton, P.H., Gaines, W.L., Keane, R.E., Aplet, G.H.,  
552 Stephens, S.L., Morgan, P., Bisson, P.A., Rieman, B.E., Salter, R.B., Reeves, G.H., 2015.  
553 Restoring fire-prone Inland Pacific landscapes: seven core principles. *Landsc. Ecol.* 30,  
554 1805–1835. <https://doi.org/10.1007/s10980-015-0218-0>
- 555 Hoff, R.M., Christopher, S.A., 2009. Remote Sensing of Particulate Pollution from Space : Have  
556 We Reached the Promised Land ? *J. Air Waste Manage. Assoc.* 59, 645–675.  
557 <https://doi.org/10.3155/1047-3289.59.6.645>
- 558 Hu, X., Waller, L.A., Al-Hamdan, M.Z., Crosson, W.L., Estes, M.G., Estes, S.M., Quattrochi,  
559 D.A., Sarnat, J.A., Liu, Y., 2013. Estimating ground-level PM<sub>2.5</sub> concentrations in the  
560 southeastern U.S. using geographically weighted regression. *Environ. Res.* 121, 1–10.  
561 <https://doi.org/10.1016/j.envres.2012.11.003>
- 562 Hu, Z., 2009. Spatial analysis of MODIS aerosol optical depth, PM<sub>2.5</sub>, and chronic coronary

- 563 heart disease. *Int. J. Health Geogr.* 8, 1–10. <https://doi.org/10.1186/1476-072X-8-27>
- 564 Hubbell, B.J., Crume, R. V., Evarts, D.M., Cohen, J.M., 2010. Policy Monitor: Regulation and  
565 progress under the 1990 Clean Air Act Amendments. *Rev. Environ. Econ. Policy* 4, 122–  
566 138. <https://doi.org/10.1093/reep/rep019>
- 567 Hystad, P., Demers, P.A., Johnson, K.C., Brook, J., Van Donkelaar, A., Lamsal, L., Martin, R.,  
568 Brauer, M., 2012. Spatiotemporal air pollution exposure assessment for a Canadian  
569 population-based lung cancer case-control study. *Environ. Heal. A Glob. Access Sci.*  
570 *Source* 11, 1–22. <https://doi.org/10.1186/1476-069X-11-22>
- 571 J.A.Gillies, W.G.Nickling, G.H.Mctainsh, 1996. Dust concentration s and particle-size  
572 characteristics of an intense dust haze event: inland delta region. *Atmos. Environ.* 30, 1081–  
573 1090.
- 574 Kearns, M., Ron, D., 1999. Algorithmic stability and sanity-check bounds for leave-one-out  
575 cross-validation. *Neural Comput.* 11, 1427–1453.  
576 <https://doi.org/10.1162/089976699300016304>
- 577 Koelemeijer, R.B.A., Homan, C.D., Matthijsen, J., 2006. Comparison of spatial and temporal  
578 variations of aerosol optical thickness and particulate matter over Europe. *Atmos. Environ.*  
579 40, 5304–5315. <https://doi.org/10.1016/j.atmosenv.2006.04.044>
- 580 Kollanus, V., Tiittanen, P., Niemi, J. V., Lanki, T., 2016. Effects of long-range transported air  
581 pollution from vegetation fires on daily mortality and hospital admissions in the Helsinki  
582 metropolitan area, Finland. *Environ. Res.* 151, 351–358.  
583 <https://doi.org/10.1016/j.envres.2016.08.003>

Xue, Gupta, Christopher, submitted to Atmospheric Chemistry and Physics

- 584 Liu, Y., Sarnat, J.A., Kilaru, V., Jacob, D.J., Koutrakis, P., 2005. Estimating ground-level PM<sub>2.5</sub>  
585 in the eastern United States using satellite remote sensing. *Environ. Sci. Technol.* 39, 3269–  
586 3278. <https://doi.org/10.1021/es049352m>
- 587 Loader, C.R., 1999. BANDWIDTH SELECTION: CLASSICAL OR PLUG-IN? *Ann. Stat.* 27,  
588 415–438.
- 589 Lyapustin, A., Korkin, S., Wang, Y., Quayle, B., Laszlo, I., 2012. Discrimination of biomass  
590 burning smoke and clouds in MAIAC algorithm. *Atmos. Chem. Phys.* 12, 9679–9686.  
591 <https://doi.org/10.5194/acp-12-9679-2012>
- 592 Lyapustin, A., Wang, Y., Korkin, S., Huang, D., 2018. MODIS Collection 6 MAIAC Algorithm.  
593 *Atmos. Meas. Tech.* 11, 5741–5765. <https://doi.org/10.5194/amt-2018-141>
- 594 Ma, Z., Hu, X., Huang, L., Bi, J., Liu, Y., 2014. Estimating ground-level PM<sub>2.5</sub> in china using  
595 satellite remote sensing. *Environ. Sci. Technol.* 48, 7436–7444.  
596 <https://doi.org/10.1021/es5009399>
- 597 Meixner, T., Wohlgemuth, P., 2004. Wildfire Impacts on Water Quality. *J. Wildl. Fire* 13, 27–  
598 35.
- 599 Melillo, J.M., Richmond, T., Yohe, G.W., 2014. Climate Change Impacts in the United States.  
600 *Third Natl. Clim. Assess.* 52. <https://doi.org/10.7930/J0Z31WJ2>.
- 601 Miao, Y., Liu, S., Guo, J., Huang, S., Yan, Y., Lou, M., 2018. Unraveling the relationships  
602 between boundary layer height and PM<sub>2.5</sub> pollution in China based on four-year radiosonde  
603 measurements. *Environ. Pollut.* 243, 1186–1195.  
604 <https://doi.org/10.1016/j.envpol.2018.09.070>

Xue, Gupta, Christopher, submitted to Atmospheric Chemistry and Physics

- 605 Miller, D.J., Sun, K., Zondlo, M.A., Kanter, D., Dubovik, O., Welton, E.J., Winker, D.M.,  
606 Ginoux, P., 2011. Assessing boreal forest fire smoke aerosol impacts on U.S. air quality: A  
607 case study using multiple data sets. *J. Geophys. Res. Atmos.* 116.  
608 <https://doi.org/10.1029/2011JD016170>
- 609 Mirzaei, M., Bertazzon, S., Couloigner, I., 2018. Modeling Wildfire Smoke Pollution by  
610 Integrating Land Use Regression and Remote Sensing Data : Regional Multi-Temporal  
611 Estimates for Public Health and Exposure Models. *Atmosphere (Basel)*. 9, 335.  
612 <https://doi.org/10.3390/atmos9090335>
- 613 Munoz-alpizar, R., Pavlovic, R., Moran, M.D., Chen, J., Gravel, S., Henderson, S.B., Sylvain,  
614 M., Racine, J., Duhamel, A., Gilbert, S., Beaulieu, P., Landry, H., Davignon, D., Cousineau,  
615 S., Bouchet, V., 2017. Multi-Year (2013–2016) PM<sub>2.5</sub> Wildfire Pollution Exposure over  
616 North America as Determined from Operational Air Quality Forecasts. *Atmosphere (Basel)*.  
617 8, 179. <https://doi.org/10.3390/atmos8090179>
- 618 Navarro, K.M., Schweizer, D., Balmes, J.R., Cisneros, R., 2018. A review of community smoke  
619 exposure from wildfire compared to prescribed fire in the United States. *Atmosphere*  
620 *(Basel)*. 9, 1–11. <https://doi.org/10.3390/atmos9050185>
- 621 Samet, J.M., 2011. The clean air act and health - A clearer view from 2011. *N. Engl. J. Med.*  
622 365, 198–201. <https://doi.org/10.1056/NEJMp1103332>
- 623 Sapkota, A., Symons, J.M., Kleissl, J., Wang, L., Parlange, M.B., Ondov, J., Breyse, P.N.,  
624 Diette, G.B., Eggleston, P.A., Buckley, T.J., 2005. Impact of the 2002 Canadian forest fires  
625 on particulate matter air quality in Baltimore City. *Environ. Sci. Technol.* 39, 24–32.  
626 <https://doi.org/10.1021/es035311z>

Xue, Gupta, Christopher, submitted to Atmospheric Chemistry and Physics

- 627 Stephens, S.L., 2005. Forest fire causes and extent on United States Forest Service lands. *Int. J.*  
628 *Wildl. Fire* 14, 213–222. <https://doi.org/10.1071/WF04006>
- 629 Trueblood, M.B., Lobo, P., Hagen, D.E., Achterberg, S.C., Liu, W., Whitefield, P.D., 2018.  
630 Application of a hygroscopicity tandem differential mobility analyzer for characterizing PM  
631 emissions in exhaust plumes from an aircraft engine burning conventional and alternative  
632 fuels. *Atmos. Chem. Phys.* 18, 17029–17045. <https://doi.org/10.5194/acp-18-17029-2018>
- 633 U.S. Environmental Protection Agency, 2019. Particulate Matter (PM2.5) Trends.
- 634 Wang, H., Shi, G., Tian, M., Zhang, L., Chen, Y., Yang, F., Cao, X., 2017. Aerosol optical  
635 properties and chemical composition apportionment in Sichuan Basin, China. *Sci. Total*  
636 *Environ.* 577, 245–257. <https://doi.org/10.1016/j.scitotenv.2016.10.173>
- 637 Xu, T., Song, Y., Liu, M., Cai, X., Zhang, H., Guo, J., Zhu, T., 2019. Temperature inversions in  
638 severe polluted days derived from radiosonde data in North China from 2011 to 2016. *Sci.*  
639 *Total Environ.* 647, 1011–1020. <https://doi.org/10.1016/j.scitotenv.2018.08.088>
- 640 You, T., Wu, R., Huang, G., Fan, G., 2017. Regional meteorological patterns for heavy pollution  
641 events in Beijing. *J. Meteorol. Res.* 31, 597–611. [https://doi.org/10.1007/s13351-017-6143-](https://doi.org/10.1007/s13351-017-6143-1)  
642 1
- 643 You, W., Zang, Z., Pan, X., Zhang, L., Chen, D., 2015. Estimating PM2.5 in Xi'an, China using  
644 aerosol optical depth: A comparison between the MODIS and MISR retrieval models. *Sci.*  
645 *Total Environ.* 505, 1156–1165. <https://doi.org/10.1016/j.scitotenv.2014.11.024>
- 646 You, W., Zang, Z., Zhang, L., Li, Y., Pan, X., Wang, W., 2016. National-scale estimates of  
647 ground-level PM2.5 concentration in China using geographically weighted regression based

Xue, Gupta, Christopher, submitted to Atmospheric Chemistry and Physics

648 on 3 km resolution MODIS AOD. Remote Sens. 8. <https://doi.org/10.3390/rs8030184>

649 Zhang, H., Hoff, R.M., Engel-Cox, J.A., 2009. The relation between moderate resolution  
650 imaging spectroradiometer (MODIS) aerosol optical depth and PM<sub>2.5</sub> over the United  
651 States: A geographical comparison by U.S. Environmental Protection Agency regions. J.  
652 Air Waste Manag. Assoc. 59, 1358–1369. <https://doi.org/10.3155/1047-3289.59.11.1358>

653 Zhang, H., Wang, Y., Hu, J., Ying, Q., Hu, X.M., 2015. Relationships between meteorological  
654 parameters and criteria air pollutants in three megacities in China. Environ. Res. 140, 242–  
655 254. <https://doi.org/10.1016/j.envres.2015.04.004>

656 Zheng, C., Zhao, C., Zhu, Y., Wang, Y., Shi, X., Wu, X., Chen, T., Wu, F., Qiu, Y., 2017.  
657 Analysis of influential factors for the relationship between PM<sub>2.5</sub> and AOD in Beijing.  
658 Atmos. Chem. Phys. 17, 13473–13489. <https://doi.org/10.5194/acp-17-13473-2017>

659 Zhu, Y., Hinds, W.C., Kim, S., Sioutas, C., 2002. Concentration and size distribution of ultrafine  
660 particles near a major highway. J. Air Waste Manag. Assoc. 52, 1032–1042.  
661 <https://doi.org/10.1080/10473289.2002.10470842>

662 Zou, B., Pu, Q., Bilal, M., Weng, Q., Zhai, L., Nichol, J.E., 2016. High-resolution Satellite  
663 Mapping of Fine Particulates Based on Geographically Weighted Regression. Ieee Geosci.  
664 Remote Sens. Lett. 13, 495–499.

665

666

667

668 Table 1. Datasets used in the study with sources.

669

	Data /Model	Sensor	Spatial Resolution	Temporal Resolution	Accuracy
1	Surface PM <sub>2.5</sub>	TEOM	Point data	daily	±5~10%
2	Mid visible aerosol optical depth (AOD)	MAIAC_ MODIS	1km	daily	66% compared to AERONET
3	Fire Radiative Power (FRP)	Terra/Aqua- MODIS	1km	daily	± 7%
4	ECMWF (Meteorological variables)		0.25 degree	hourly	

670 1) <https://www.epa.gov/outdoor-air-quality-data>

671 2) <https://earthdata.nasa.gov/>

672 3) <https://earthdata.nasa.gov/>

673 4) <https://www.ecmwf.int/en/forecasts>

674

675

676

677 Table 2. Total FRP in Canada and Northwestern US in August of Different Years (unit:  $10^4$

678 MW)

Year	2010	2011	2012	2013	2014	2015	2016	2017	2018
CA	148.24	4.84	19.93	70.54	107.78	10.39	4.6	307.3	542.99
NW US	16.41	42.84	320.39	192.06	67.01	339.58	112.9	195.64	296.91

679

680 Table 3. statistics of 15 states that violate EPA standards ( $35 \mu g m^{-3}$ ) during the 17-day wildfire  
681 period

State	number of site violate standard	number of site in the state	Percentage of site violate standard (%)	number of days violate standard
Montana	14	15	93.34	16
Washington	18	20	90	16
Oregon	12	14	85.71	5
North Dakota	7	11	63.63	4
Idaho	5	8	62.5	8
Colorado	11	21	52.38	2
South Dakota	5	10	50	1
California	57	119	47.9	14
Utah	7	15	46.67	4
Nevada	4	13	30.77	1
Wyoming	7	24	29.2	2
Minnesota	4	26	15.4	2
Texas	3	37	8.1	1
Louisiana	1	14	7.1	1
Arizona	1	20	5	1

682

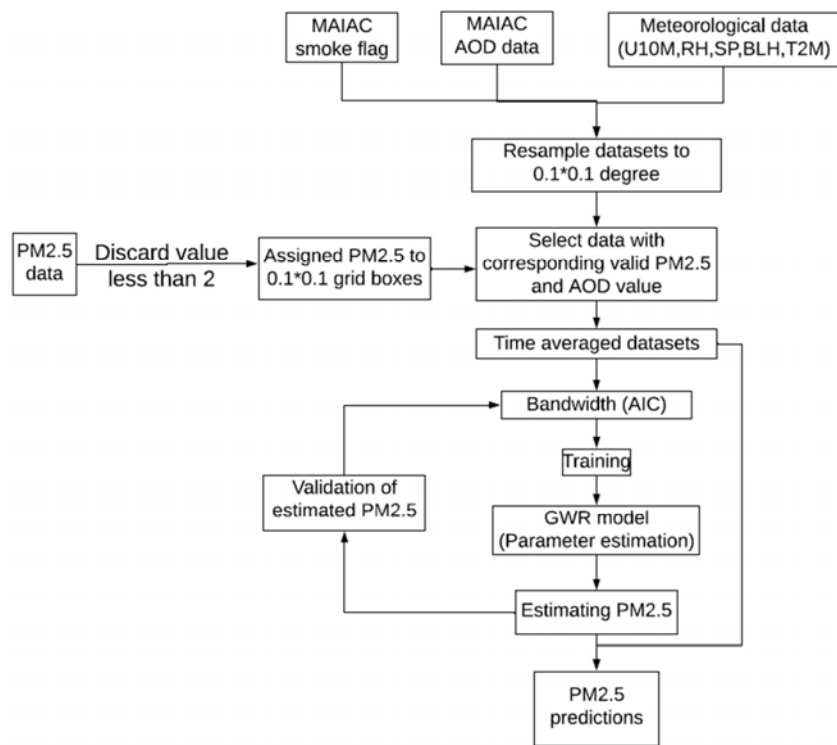
683 Table 4. Coefficients of different predictors

Mean coefficients	sample selection	N	AOD	smoke flag	PBL	T2M	RH	U	SP
box1(red)	FRP>1000	213	91.94	-0.14	-2.25	0.33	0.08	-2	-0.06
box2(gold)	PM2.5>30	362	60.1	0.013	-2.9	0.23	-0.08	-1.6	-0.03
box3(green)	PM2.5>17	278	6.2	0.05	0.2	0.2	0.014	-0.3	-0.02
box4(black)	17>PM2.5>10	938	7.1	-0.02	-1.2	0.22	-0.035	0.06	-0.005
whole US region	~	106352	28.1	0.024	-0.9	0.06	-0.04	-0.7	-0.002



684

685



686

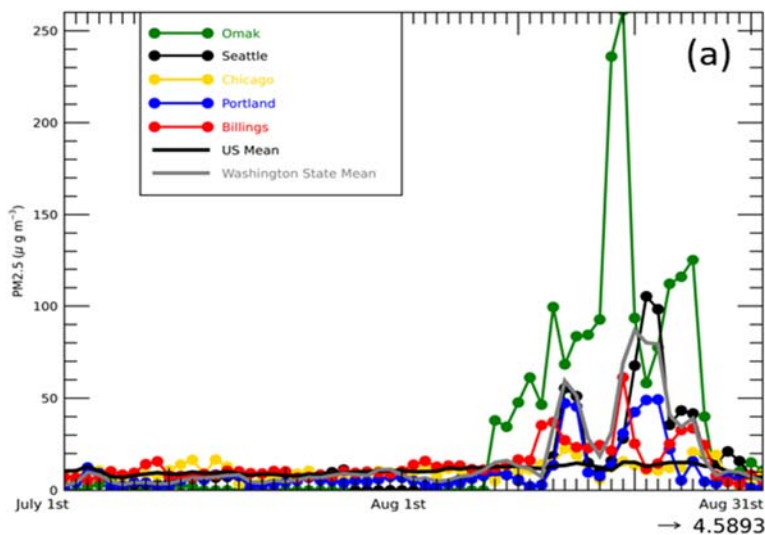
687 Figure 1. Flow chart for the Geographically Weighted Regression model used. All satellite,

688

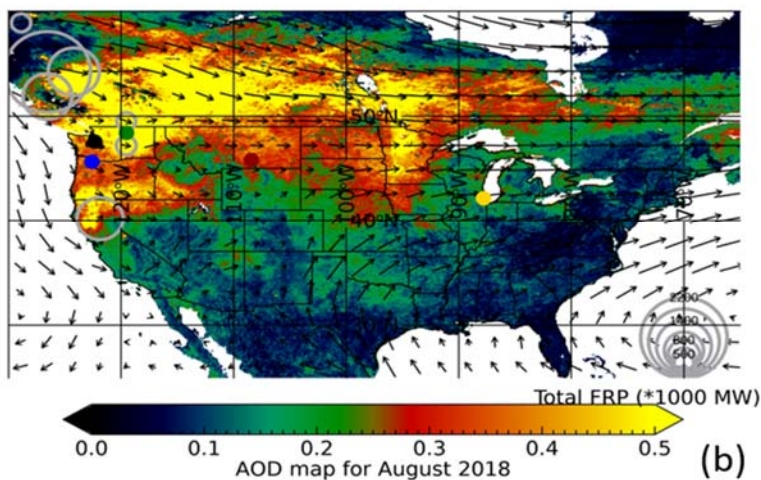
ground, meteorological data are gridded to 0.1 by 0.1 degrees.

689

690

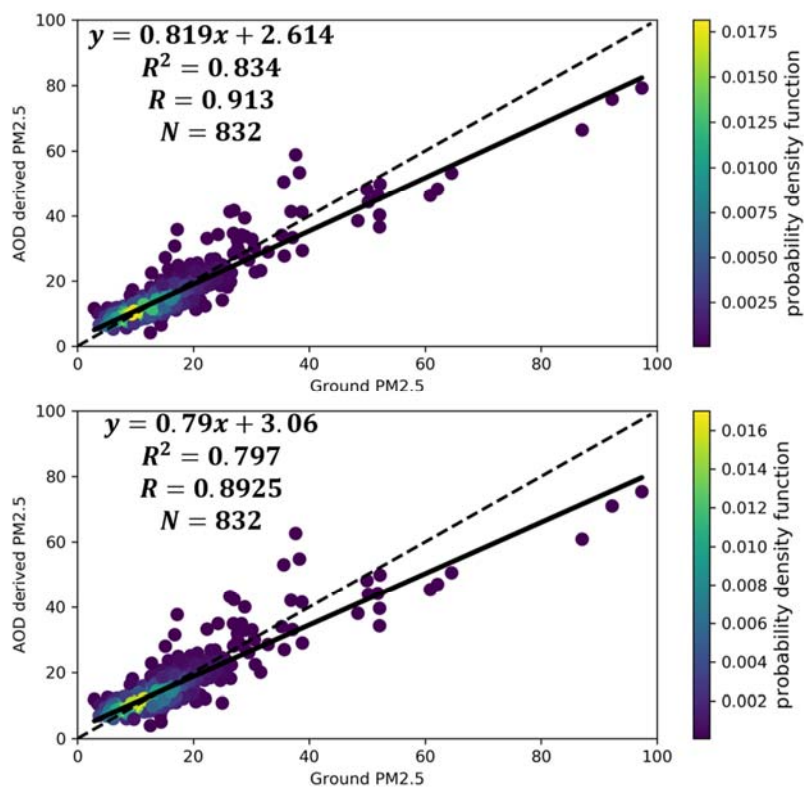


691



692

693 Figure 2. (a) Variations of EPA ground observed  $PM_{2.5}$  in different cities from July to August  
 694 2018 (Omak-Washington, Seattle-Washington, Chicago-Illinois, Portland-Oregon, Billings-  
 695 Montana). Black line without markers shows the mean variation of the whole US stations and the  
 696 grey line without markers shows the mean variation of stations in Washington state. (b) Mean  
 697 MAIAC satellite AOD distribution from August 9th to August 25th, 2018. AOD values equal or  
 698 larger than 0.5 are shown as the same color (yellow). Also shown are circles with Fire Radiative  
 699 Power (FRP). Black arrow shows the wind direction and the length of it represents the wind  
 700 speed. The round spots of different colors on the map show the locations of the five selected  
 701 cities (green-Omak, black-Seattle, yellow-Chicago, blue-Portland, red-Billings).



702

703 Figure 3. Results of model fitting and cross validation for GWR model for the entire US region  
704 averaged from August 9th to August 25th, 2018. (a) GWR model fitting results (b) GWR model  
705 LOOCV results. The dash line is the 1:1 line as reference and the black line shows the regression  
706 line. The color of the scatter plots represents the probability density function which provides a  
707 relative likelihood that the value of the random variable would equal a certain sample.

708

709

710

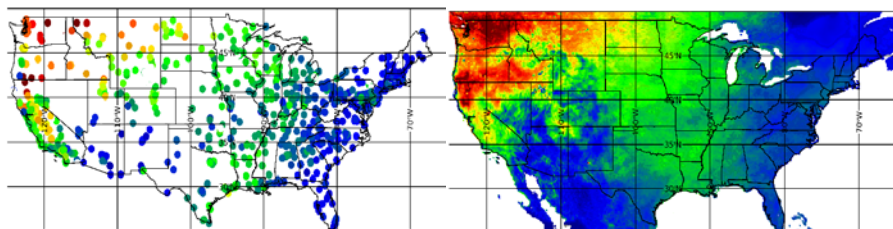
711

712

713

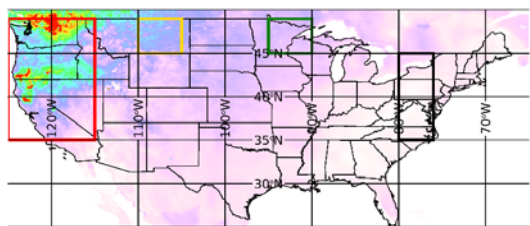
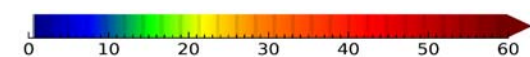
714

715



716

717

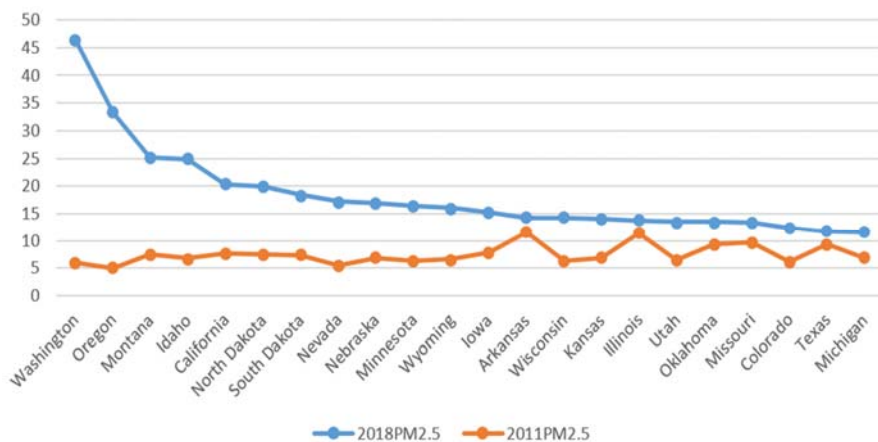


D-PM2.5 map between 2018 and 2011 August

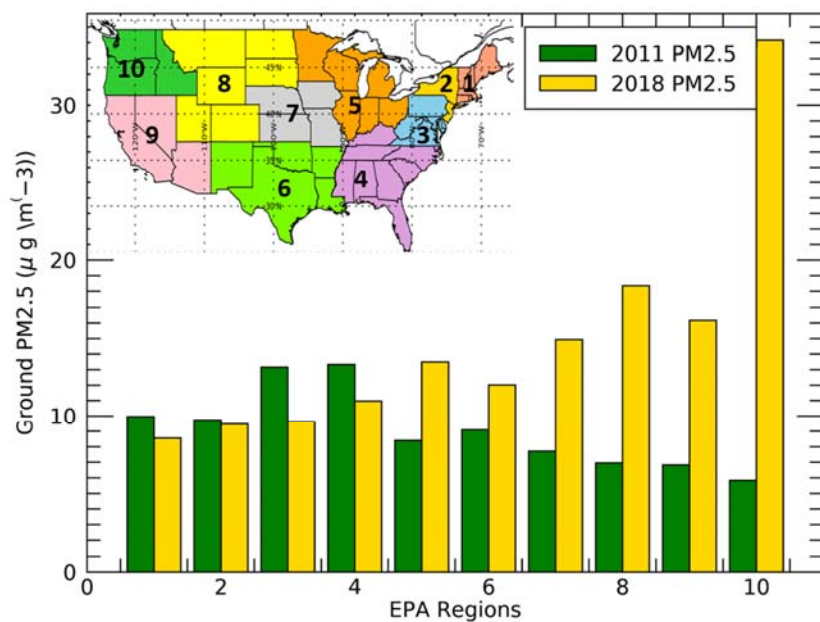
718

719 Figure 4. (a) EPA ground observed  $PM_{2.5}$  distribution over the US averaged from August 9th to  
720 August 25th, 2018. (b) GWR predicted 17-day mean  $PM_{2.5}$  distribution. (c) Difference map of  
721 predicted ground  $PM_{2.5}$  of the 17-day mean values between 2018 and 2011.  $PM_{2.5}$  values equal or  
722 larger than  $60 \mu g m^{-3}$  are shown as the same color (red). Note that the D- $PM_{2.5}$  has a different  
723 color scale to make the negative values more apparent (blue).  
724

725



726  
727 Figure 5. Mean PM<sub>2.5</sub> from August 9<sup>th</sup> to August 25<sup>th</sup> in 2018 and 2011 of most affected states  
728  
729



730

731 Figure 6. Mean PM<sub>2.5</sub> of EPA regions from August 9th to August 25th in 2011 and 2018. Inset  
732 shows the map of 10 EPA regions in different colors. Yellow column represents the 2018 mean  
733 PM<sub>2.5</sub> and green column represents for 2011 mean PM<sub>2.5</sub>.

734

735